JCB Journal of Cell Biology

REPORT

Coupling of Cdc20 inhibition and activation by BubR1

Jamin B. Hein[1], Dimitriya H. Garvanska[1], Isha Nasa[2], Arminja N. Kettenbach[2], and Jakob Nilsson[1]

Tight regulation of the APC/C-Cdc20 ubiquitin ligase that targets cyclin B1 for degradation is important for mitotic fidelity. The spindle assembly checkpoint (SAC) inhibits Cdc20 through the mitotic checkpoint complex (MCC). In addition, phosphorylation of Cdc20 by cyclin B1–Cdk1 independently inhibits APC/C–Cdc20 activation. This creates a conundrum for how Cdc20 is activated before cyclin B1 degradation. Here, we show that the MCC component BubR1 harbors both Cdc20 inhibition and activation activities, allowing for cross-talk between the two Cdc20 inhibition pathways. Specifically, BubR1 acts as a substrate specifier for PP2A-B56 to enable efficient Cdc20 dephosphorylation in the MCC. A mutant Cdc20 mimicking the dephosphorylated state escapes a mitotic checkpoint arrest, arguing that restricting Cdc20 dephosphorylation to the MCC is important. Collectively, our work reveals how Cdc20 can be dephosphorylated in the presence of cyclin B1-Cdk1 activity without causing premature anaphase onset.

Introduction

Proper progression through mitosis depends on tight regulation of the Cdc20 protein, which is an activator of the anaphase-promoting complex/cyclosome (APC/C), a large E3 ubiquitin ligase (Alfieri et al., 2017; Barford, 2020). The APC/C–Cdc20 complex targets several proteins for proteasomal degradation, including cyclin B1 and securin, which initiate anaphase by lowering Cdk1 kinase activity and releasing centromere cohesion, respectively (Pines, 2011). Cdc20 activity is regulated by the spindle assembly checkpoint (SAC), which, in response to unattached kinetochores, delays anaphase onset by promoting the assembly of the mitotic checkpoint complex (MCC; Lara-Gonzalez et al., 2012; Musacchio, 2011; Varetti and Musacchio, 2008). The MCC is composed of Mad2-Cdc20-BubR1-Bub3, where Cdc20 is tightly bound and critical surface areas responsible for APC/C activation are blocked (Chao et al., 2012; Di Fiore et al., 2015; Di Fiore et al., 2016; Herzog et al., 2009; Sudakin et al., 2001). The kinetochore-generated MCC complex binds stably to the APC/C–Cdc20 complex to generate an APC/C–MCC complex containing two Cdc20 molecules (Alfieri et al., 2016; Hein and Nilsson, 2014; Izawa and Pines, 2015; Primorac and Musacchio, 2013; Yamaguchi et al., 2016).

In addition to SAC regulation of Cdc20, we and others have shown that cyclin B1–Cdk1 can phosphorylate a number of Thr-Pro (TP) sites in the N-terminal region of Cdc20 to block its activity (Hein et al., 2017; Hein and Nilsson, 2016; Labit et al., 2012; Yudkovsky et al., 2000). These phosphorylation sites cluster around the C-box of Cdc20, a motif that binds and activates the APC/C (Chang et al., 2014; Kimata et al., 2008). For activation of Cdc20, TP sites must be dephosphorylated (Labit et al., 2012). We previously showed that the PP2A-B55 phosphatase is able to do so in vitro and in human cells (Hein et al., 2017). PP2A-B55 is a Ser/Thr phosphatase that is specifically activated at the metaphase–anaphase transition to dephosphorylate thousands of Cdk1 targets, thereby driving the anaphase transition (Cundell et al., 2016; Godfrey et al., 2017; Holder et al., 2019; Kruse et al., 2020; McCloy et al., 2015; Nilsson, 2019). PP2A-B55 activity is regulated by the Cdk1-MASTL-ARPP19 pathway in which Cdk1 activates the MASTL kinase that then phosphorylates ARPP19/ENSA proteins, which bind and inactivate PP2A-B55 (Gharbi-Ayachi et al., 2010; Mochida et al., 2010; Vigneron et al., 2009). The activation of PP2A-B55 is initiated by a decrease in Cdk1 activity, which activates PP1 to initiate dephosphorylation and inactivation of the MASTL kinase (Heim et al., 2015; Ma et al., 2016; Rogers et al., 2016).

This generates a conundrum because Cdc20 needs to be dephosphorylated before PP2A-B55 can become active. One solution to this problem could be that another protein phosphatase activates Cdc20 before PP2A-B55, but this would potentially lead to premature activation of Cdc20 and deregulation of cell division. Here, we provide experimental evidence showing that both PP2A-B55 and PP2A-B56 are phosphatases for Cdc20. PP2A-B56 is active in prometaphase and, through binding to BubR1, it selectively dephosphorylates Cdc20 within the MCC, thereby

[1]Novo Nordisk Foundation Center for Protein Research, Faculty of Health and Medical Science, Copenhagen, Denmark; [2]Biochemistry and Cell Biology, Geisel School of Medicine at Dartmouth College, Hanover, NH.

Correspondence to Jakob Nilsson: jakob.nilsson@cpr.ku.dk.

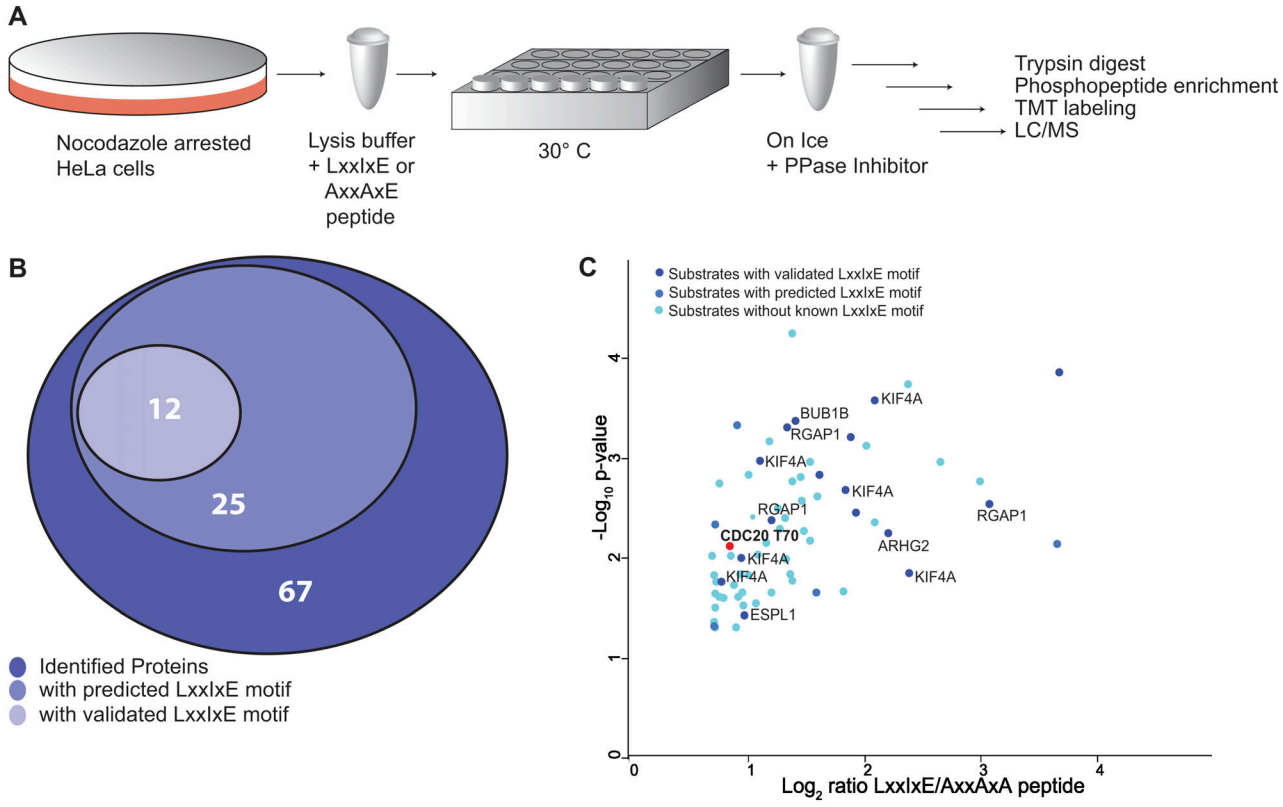

D

Name	Modsites	LxxIxE/AxxAxE	pvalue	LxxIxE
KIF4A	T799	2.09	0.00	Yes
RGAP1	S203	1.42	0.00	Yes
ESPL1	S1475	0.98	0.03	Yes
ARHG2	S886	2.22	0.00	Yes
BUB1B	T508	1.35	0.00	Yes
ADA17	T735	0.92	0.00	Yes
⋮	⋮	⋮	⋮	⋮
KIF2C	S95	3.67	0.00	Predicted
KIF4B	S1038	3.68	0.00	Predicted
RIF1	S1008	1.46	0.00	Predicted
ZC11A	S290	1.28	0.01	Predicted
⋮	⋮	⋮	⋮	⋮

E

Name	Modsites	LxxIxE/AxxAxE	pvalue	LxxIxE
LAP2B	T279	2.39	0.00	No
SCRIB	S1508	3.00	0.00	No
REPI1	T287	2.09	0.00	No
REPI1	T482	2.02	0.00	No
CDK17	S180	1.55	0.00	No
REPI1	T510	1.39	0.03	No
CDK18	S89	1.48	0.00	No
PHF14	S290	1.37	0.01	No
NAB1	S103	1.34	0.02	No
SYMPK	S494	1.27	0.01	No
⋮	⋮	⋮	⋮	⋮
CDC20	T70	0.85	0.02	No

Figure 1. **A screen for mitotic PP2A-B56 substrates identifies Cdc20. (A)** A schematic of the approach used to identify PP2A-B56 substrates in nocodazole arrested cells. **(B)** Summary of the screen results categorizing sites based on the presence of validated or predicted LxxIxE motifs. **(C)** Log2 ratio of regulated phosphorylation sites versus P value. Sites in proteins with validated LxxIxE motifs are indicated with protein names as well as Cdc20 T70. **(D and E)** Examples of identified sites in the screen and whether they contain validated, predicted, or no LxxIxE motifs. The protein name is indicated followed by the specific phosphorylation site detected and found to be regulated. The log2 ratio of B56 inhibited sample (LxxIxE peptide) vs. control-treated sample (AxxAxE) is indicated followed by the P value, calculated using a two-tailed Student's *t* test assuming unequal variance. LC/MS, liquid chromatography-mass spectrometry.

priming the inhibited pool of Cdc20 for APC/C activation before PP2A-B55 activation.

Results and discussion

A screen for PP2A-B56 mitotic substrates identifies Cdc20

We recently developed a method to identify substrates of specific protein phosphatases during mitosis (Fig. 1 A; Kruse et al., 2020). Briefly, nocodazole arrested cells are harvested and lysed in the presence of a specific inhibitor of a protein phosphatase. As ATP is rapidly depleted, this inactivates kinases while protein phosphatases are still active unless an inhibitor is present. The lysis reaction is then incubated at 30 degrees for 5 min and then the reaction is stopped. Proteins are precipitated and digested with trypsin, followed by phosphopeptide enrichment and analysis by liquid chromatography–tandem mass spectrometry. For specific inhibition of PP2A-B56, we employed a high-affinity LxxIxE motif–containing peptide that prevents the phosphatase from binding to all of its substrates (Hertz et al., 2016; Kruse et al., 2018; Kruse et al., 2020). As a control, we used an AxxAxE peptide that does not bind the phosphatase. This screen identified 54 phosphorylation sites that significantly increased (log2 ratio LxxIxE/AxxAxE > 0.7; $P < 0.05$) in lysates treated with LxxIxE peptide versus AxxAxE peptide (Fig. 1, B and C; Data S1).

Several of the regulated sites were in proteins already known to be PP2A-B56 substrates that contain validated LxxIxE motifs (Fig. 1 D). As an example, Kif4A T799 and ADAM17 T735 are known targets of PP2A-B56 and these two proteins contain validated LxxIxE motifs (Bastos et al., 2014; Kruse et al., 2020; Wang et al., 2020). Furthermore, RacGAP1 S203, BubR1 T508, and ESPL1 S1475 are close to validated LxxIxE motifs, supporting the strength of the screening approach. In addition, we identified PP2A-B56 regulated phosphorylation sites in proteins containing bioinformatically predicted LxxIxE motifs as well as proteins with no motifs (Fig. 1 E). One phosphorylation site that caught our attention was Cdc20 T70, a Cdk1 phosphorylation site known to block Cdc20 activation of the APC/C. We have previously found this phosphorylation site to be a substrate of PP2A-B55 (Hein et al., 2017), so we decided to investigate in more detail the role of PP2A-B56 in regulating this site.

Two distinct mitotic PP2A complexes can dephosphorylate Cdc20

We first confirmed that PP2A-B56 can regulate Cdc20 T70 phosphorylation in cells. We depleted all B56 regulatory subunits, arrested cells in nocodazole, immunopurified Cdc20, and analyzed T70 phosphorylation levels by quantitative Western blotting (Li-Cor Biosciences; Fig. 2 A and Fig. S1 A). Indeed, we observed increased levels of Cdc20 T70 in nocodazole arrested cells when B56 subunits were depleted. The level of copurifying APC3 and its phosphorylation on T447, a Cdk1 site, were not affected by B56 depletion. We then treated cells with the Cdk1 inhibitor, RO3306, to determine if PP2A-B56 was required for Cdc20 T70 dephosphorylation when cells exit mitosis; however, we observed efficient dephosphorylation in the absence of PP2A-B56, arguing that other protein phosphatases can dephosphorylate Cdc20 T70 (Fig. 2 A).

To investigate this, we turned to the lysate system, where we can add specific phosphatase inhibitors for a short time, avoiding indirect effects from long-term perturbation by siRNA depletion. We analyzed Cdc20 T70 phosphorylation and compared this to APC3 T447 phosphorylation in the presence of specific phosphatase inhibitors. We used thiophosphorylated Arpp19 to inhibit PP2A-B55, Nipp1 to inhibit PP1 (Winkler et al., 2015), and the LxxIxE peptide to inhibit PP2A-B56. This experiment revealed that both Arpp19 and LxxIxE, but not the corresponding controls, delayed Cdc20 T70 dephosphorylation (Fig. 2 B). In contrast, APC3 T447 dephosphorylation was only inhibited by Arpp19 (Fig. 2 C). Strikingly, the addition of both Arpp19 and LxxIxE peptide was required to strongly block Cdc20 T70 dephosphorylation. This shows that both PP2A-B55 and PP2A-B56 are able to dephosphorylate Cdc20 T70, which explains how Cdc20 gets dephosphorylated in cells depleted of PP2A-B56 upon addition of a Cdk1 inhibitor. We also confirmed that Cdc20 T59 was dephosphorylated by PP2A-B56, arguing that likely all three TP sites in Cdc20 are targeted by PP2A-B56 (Fig. S1 B).

The results show that two distinct PP2A complexes can dephosphorylate Cdc20, with PP2A-B56 likely acting during prometaphase and PP2A-B55 during anaphase.

BubR1 acts as a substrate specifier for PP2A-B56 to dephosphorylate Cdc20

Our data argue that Cdc20 T70 dephosphorylation is dependent on PP2A-B56 binding to an LxxIxE motif. This is consistent with the in vitro dephosphorylation data we recently published with which we showed that Cdc20 inhibitory Cdk1 phosphorylations can be dephosphorylated by PP2A-B56 when an LxxIxE motif is fused to Cdc20 (Kruse et al., 2020). Although PP2A-B56 works inefficiently on Cdk1 sites, the presence of LxxIxE motifs can overcome this inefficiency by positioning the phosphatase in the proximity of the Cdk1 sites.

To establish the relevant LxxIxE motif for PP2A-B56–mediated Cdc20 dephosphorylation in cells, we focused on proteins known to bind Cdc20. BubR1 contains a functional LxxIxE motif (L669-E674) and, through its N terminus, BubR1 binds tightly to the C-terminal WD40 domain of Cdc20 (Fig. 3 A). We therefore investigated whether PP2A-B56 bound to BubR1 could be responsible for Cdc20 T70 dephosphorylation. We used stable HeLa cell lines expressing siRNA-resistant Venus-tagged BubR1 WT and L669A/I672A (BubR1 2A) and immunopurified Cdc20 from these (Kruse et al., 2013). The parental cell line or the cell lines expressing exogenous BubR1 were treated with BubR1 RNAi and arrested in mitosis using nocodazole. (Of note, there is some slippage from the mitotic arrest in the samples expressing exogenous BubR1.) The level of Cdc20 T70 and APC3 T447 phosphorylation was then determined by quantitative immunoblotting (Fig. 3 B). In the purifications from Venus BubR1 2A–expressing cells, we observed a specific increase in Cdc20 T70 levels, while APC3 T447 levels were similar to those of BubR1 WT. This experiment shows that the binding of PP2A-B56 to BubR1 is important for Cdc20 dephosphorylation.

These results raised the possibility that Cdc20 as part of the MCC would be specifically dephosphorylated by PP2A-B56. To test this model, we immunopurified different Cdc20 pools from nocodazole arrested cells (Fig. 3 C). We purified total Cdc20 using two different antibodies (reflecting free Cdc20 and MCC bound Cdc20) as well as Cdc20 associated with BubR1 and APC/C (reflecting MCC and APC/C-MCC complexes). Compared with total Cdc20, we observed less Cdc20 T70 phosphorylation in BubR1 and APC4 purifications, in line with our results for Venus BubR1 2A. The degree of APC3 T447 phosphorylation was similar in all samples, arguing for a specific effect on Cdc20.

Collectively, these results show that BubR1-bound PP2A-B56 can dephosphorylate Cdc20 T70. This selective dephosphorylation leads to lower Cdc20 T70 phosphorylation in MCC and APC/C-MCC complexes.

Cdk1 phosphorylation of Cdc20 is required for a prolonged mitotic arrest

Our results support a model in which Cdc20 is selectively dephosphorylated as part of the MCC complexes. This raised the question of whether dephosphorylation of Cdc20 not inhibited by MCC would result in premature activation of APC/C–Cdc20. To investigate this, we analyzed the effect of expressing a variant of Cdc20 (Cdc20 3AA–T70, T59, and T55 mutated to AA) that cannot be phosphorylated by Cdk1 on a nocodazole-induced mitotic arrest (Hein et al., 2017). Cells stably expressing YFP-tagged

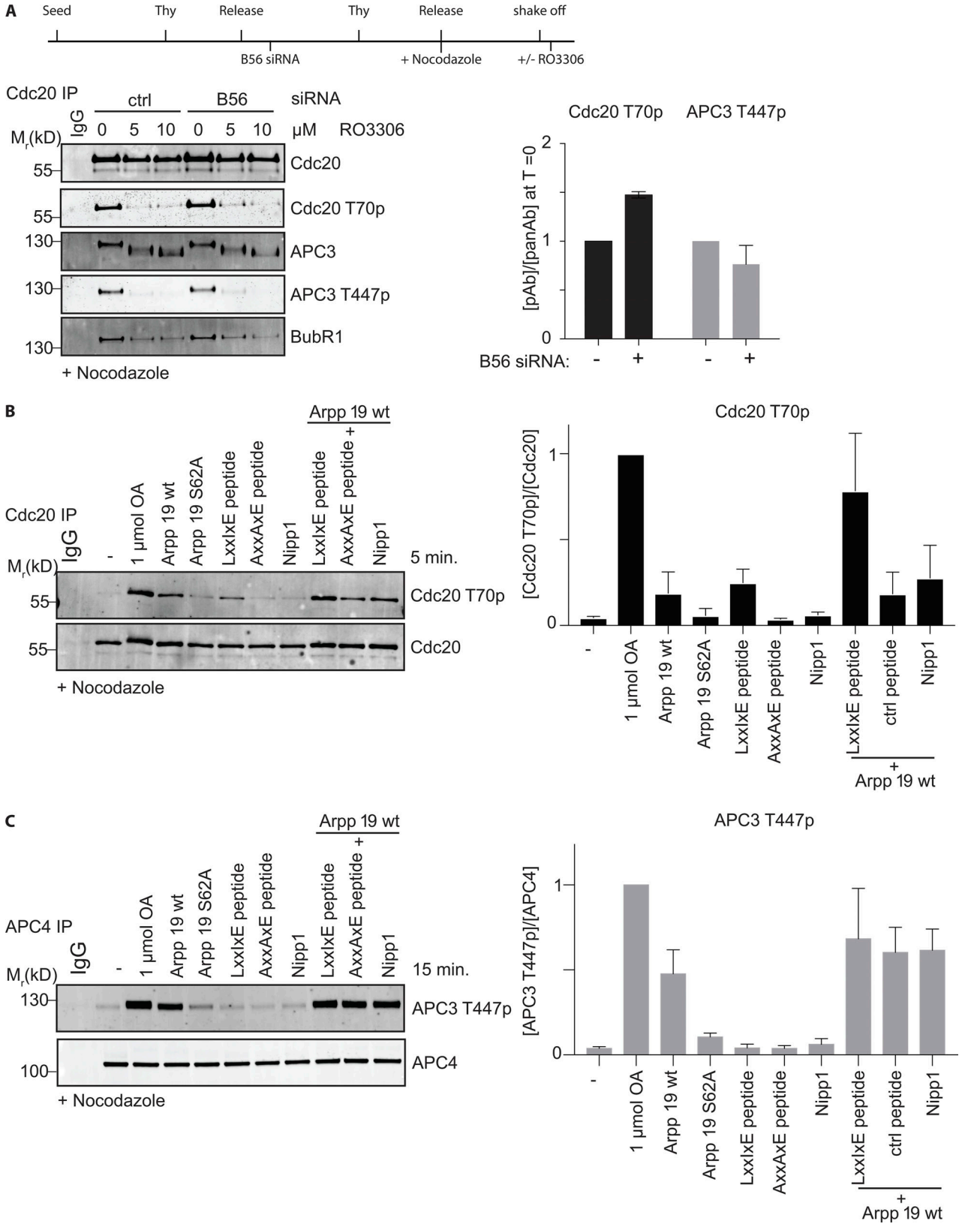

Figure 2. **PP2A-B56 and PP2A-B55 are phosphatases for Cdc20 T70. (A)** Cells treated with a control RNAi oligo or a pool of B56 RNAi oligoes targeting all isoforms were arrested in nocodazole and Cdc20 immunopurified. Samples were analyzed by Western blot for Cdc20 T70p and APC3 T447p as well as APC3 and BubR1. The degree of Cdc20 T70p and APC3 T447p was determined by normalizing to pan-Cdc20 or pan-APC3 signals. **(B and C)** A nocodazole lysate was prepared and treated with the indicated phosphatase inhibitors (see also Fig.1 A) for 5 or 15 min as indicated. Cdc20 or APC4 was immunopurified and the level of Cdc20 T70p and APC3 T447p determined. For all experiments, three independent experiments were conducted and quantified. Ctrl, control.

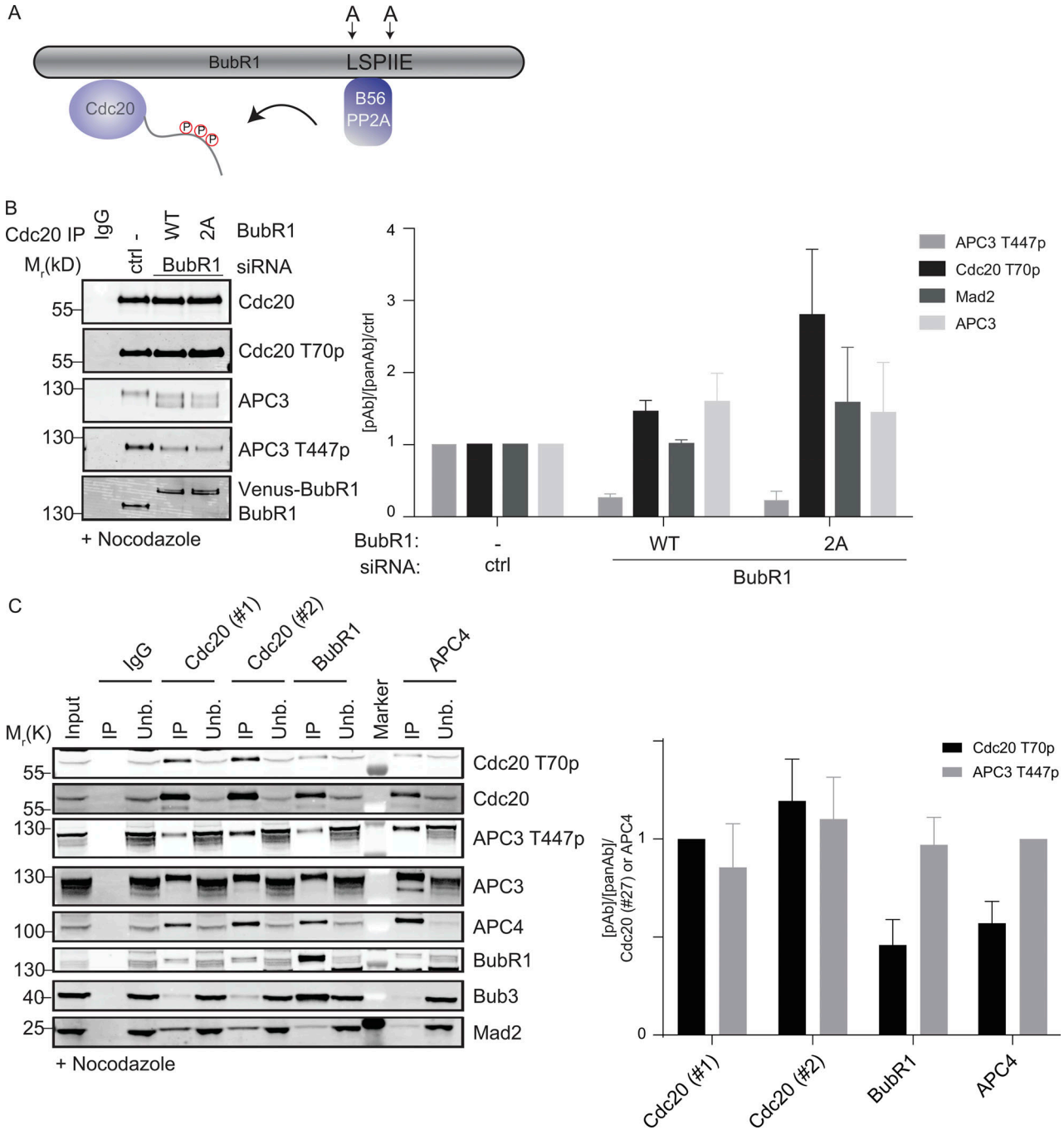

Figure 3. **Cdc20 T70 is dephosphorylated by BubR1 bound PP2A-B56. (A)** Schematic indicating Cdc20 and PP2A-B56 binding to BubR1. The mutations in BubR1 2A are indicated. **(B)** Stable cell lines expressing Venus-BubR1 WT or 2A were depleted of BubR1 by RNAi and arrested in mitosis with nocodazole. Cdc20 was immunopurified from the cells and the degree of Cdc20 T70p and APC3 T447p determined. Samples were compared with similar samples from the parental cells not treated with BubR1 RNAi. **(C)** Cdc20, BubR1, and APC4 were immunopurified from nocodazole arrested cells and the level of Cdc20 T70p and APC3 T447p determined. The signal from the phosphospecific antibody was normalized to the pan-specific antibody for Cdc20, and for APC3 T447p the signal was normalized to APC4. For Cdc20, two different antibodies were used. For all experiments, at least three independent experiments were conducted and quantified. Ctrl, control.

or untagged Cdc20 variants were depleted of endogenous Cdc20 and followed by time-lapse microscopy (Fig. 4, A and B; and Fig. S1, C–E). Strikingly, a large fraction of Cdc20 3AA–expressing cells escaped the mitotic arrest while Cdc20 WT and Cdc20 3DD stayed arrested. We further analyzed the effect of Cdk1 phosphorylation of Cdc20 using mutants of Cdc20 that cannot form the MCC (Cdc20 R132A and 4A; Lischetti et al., 2014). With both of these Cdc20 mutants, we observed a faster exit when Cdk1 phosphorylation was prevented (Fig. 4, C and D). This argues that Cdk1 phosphorylation of Cdc20 contributes to maintaining a mitotic arrest independently of the SAC.

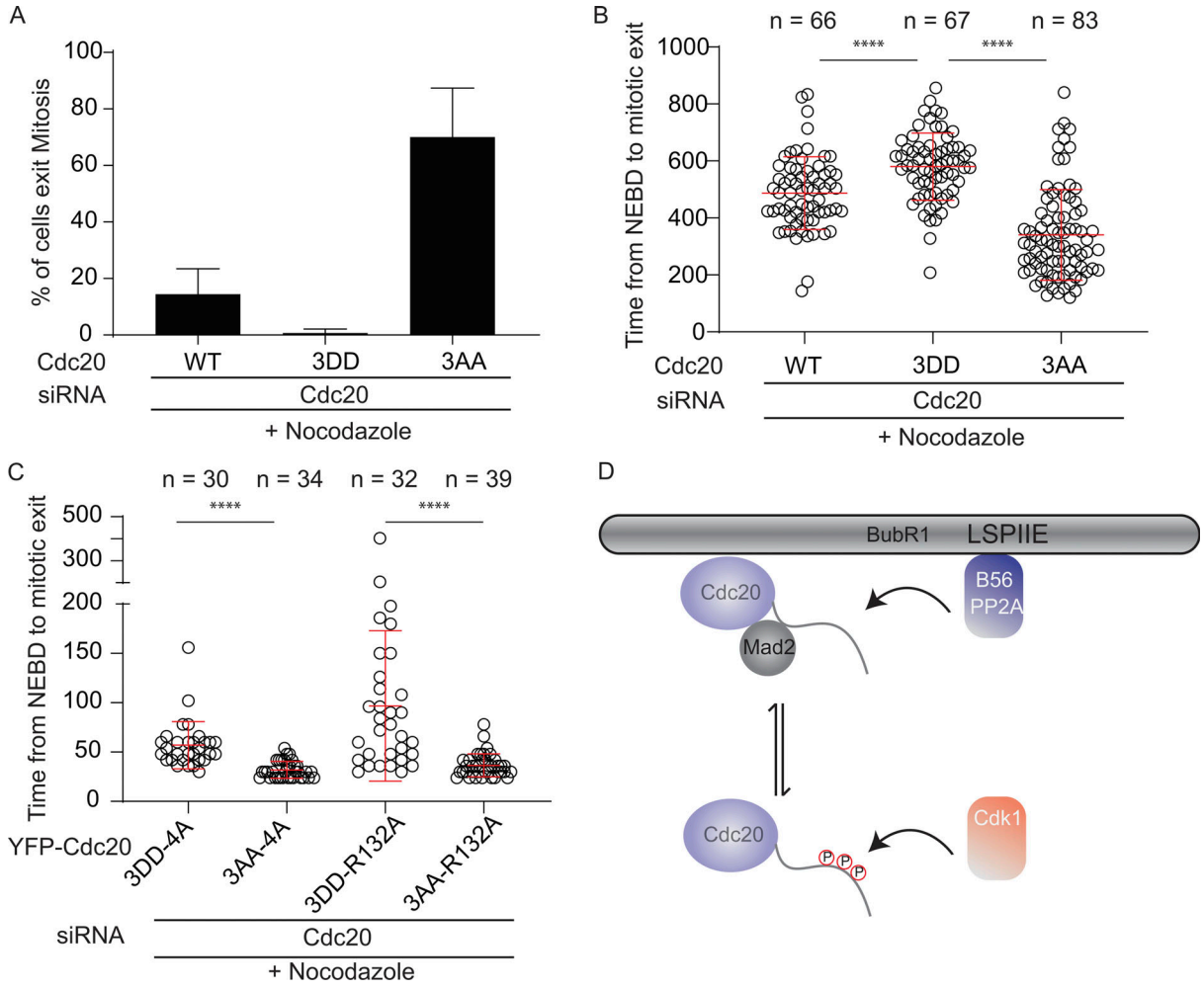

Figure 4. **Cdk1 phoshorylation of Cdc20 is required for an efficient mitotic arrest in response to microtubule poisons. (A)** Live cell imaging of Hela cells depleted of endogenous Cdc20 and transiently expressing untagged Cdc20 WT, 3DD, or 3AA in the presence of nocadazole (30 ng/ml). Percentage of cells that exit mitosis during the course of imaging from three independent experiments (mean and SD indicated). **(B)** As in A, time from nuclear envelope breakdown (NEBD) to mitotic exit or end of filming from three independent experiments (each dot represents a single cell, red line indicates mean and SD, *n* values are shown in the graph and represent single cells analyzed per condition; statistical analysis with Mann-Whitney test; ****P > 0.0001). **(C)** Live cell imaging of stable cell lines that were depleted of endogenous Cdc20 and expressing indicated YFP-tagged Cdc20 proteins in the presence of nocodazole (30 ng/ml). The R132A mutation prevents Mad2 binding, while the 4A mutations prevent BubR1 binding. Time from NEBD to mitotic exit (each dot represents a single cell, red line indicates mean and standard deviation, *n* values are shown in the graph and represent single cells analyzed per condition, statistical analysis with Mann-Whitney test; ****P > 0.0001). **(D)** Model: MCC-bound BubR1 is preferentially dephosphorylated by PP2A-B56, whereas free Cdc20 is phosphorylated by Cdk1.

In summary, our work explains how Cdc20 can be dephosphorylated even in the presence of high levels of cyclin B1–Cdk1. By coupling Cdc20 dephosphorylation to an MCC component, this ensures that dephosphorylated Cdc20 is kept inactive but ready to activate the APC/C once the SAC is satisfied. At present, we do not know if PP2A-B56 bound to BubR1 can act on both Cdc20 molecules in the APC/C–MCC complex. If this is the case, this could ensure that, once the MCC dissociates, the APC/C–Cdc20 complex is fully active. Our data also suggest that Cdc20 phosphorylation prevents unscheduled activation during a mitotic arrest, possibly by inactivating Cdc20 not bound to MCC components. Recent work from the Yamano laboratory using *Xenopus laevis* embryonic extracts identified PP2A-B56 as a Cdc20 phosphatase, consistent with our work (Fujimitsu and Yamano, 2020). Their work showed that an LxxIxE motif in APC1 binds to PP2A-B56 to mediate efficient Cdc20 binding, although the level of Cdc20 phosphorylation was not analyzed. We have not explored this motif, but since the *X. laevis* extract lacks a functional SAC, BubR1 cannot act as a substrate specifier for PP2A-B56 in this system. We note that APC1 mutants that cannot bind PP2A-B56 progress with almost WT kinetics into anaphase, which suggests that another phosphatase can activate Cdc20. Based on our results, we believe that this is PP2A-B55. A recent study also implicated PP1 in Cdc20 T70 dephosphorylation in human cells, in line with work from *Caenorhabditis elegans* showing PP1 as a Cdc20 phosphatase (Bancroft et al., 2020; Kim et al., 2017). The results from human somatic cells could be an indirect effect of PP1 inhibition, leading to delayed PP2A-B55 activation. In our lysate experiment, we saw no effect on Cdc20 T70 phosphorylation upon PP1 inhibition by Nipp1. In agreement with this, depletion of PP1α/γ showed limited effect on Cdc20 T70 dephosphorylation in cells (Bancroft et al., 2020);

however, further work is needed to clarify if PP1 can dephosphorylate Cdc20 in cells.

We posit that, in the absence of PP2A-B56, mitotic exit through Cdc20 dephosphorylation is possible and can be driven by PP2A-B55. This redundancy in Cdc20 phosphatases can explain the limited effect on a forced mitotic exit in cells expressing BubR1 that are unable to bind PP2A-B56 (Espert et al., 2014; Nijenhuis et al., 2014); however, in unperturbed conditions, Cdc20 dephosphorylation by BubR1-PP2A-B56 is likely required for efficient onset of anaphase, allowing a drop in cyclin B1 levels and thus PP2A-B55 activation. This activation of PP2A-B55 would then further activate APC/C–Cdc20 to ensure a rapid metaphase–anaphase transition.

Collectively, our work provides important insight into the regulation of Cdc20 and reveals that BubR1 integrates both inhibitory and activating activities.

Materials and methods

Cloning

The cloning was performed as previously described in Hein et al. (2017). In short, full-length Cdc20 was amplified by PCR and cloned into the BamHI and NotI sites of pcDNA5/FRT/TO 3*FLAG-Venus. Synthetic DNA corresponding to the first 344 nucleotides of Cdc20 with T55, T59, and T70 changed to either alanine (3AA) or aspartic acid (3DD) was ordered from GeneArt and assembled by two-step PCR and cloned into BamHI and NotI sites of pcDNA5/FRT/TO 3*FLAG-Venus. The Cdc20 sequence was made resistant to the Cdc20 RNAi oligo by introducing silent mutations by quick-change PCR. Cdc20 R132A and 4A was introduced into Cdc20 3AA and 3DD using quick-change PCR (R132A: 5′-GCCAAGATCCTTGCGCTCAGTGGAAAAC-3′ and 5′-GTTTTCCACTGAGCGCAAGGATCTTGGC-3′; and 4A: 5′-AACAGGAGGGGGCGCCGCTGCTGCACACATTCGCATCTG-3′ and 5′-CAGATGCGAATGTGTGCAGCAGCGGCGCCCCCTCCTGTT-3′). RNAi-resistant Cdc20 WT, 3AA, and 3DD was cloned into Xho1 and BamH1 site of pIRES-AcGFP1 (Clonetech).

BubR1 WT and 2A are described in Kruse et al. (2013), and Cdc20 R132A and 4A are described in Lischetti et al. (2014).

Antibodies

The following antibodies were used at the indicated dilutions for Western blot: Cdc20 mouse monoclonal antibody (1:1,000; sc-13162; Santa Cruz Biotechnology; clone E7, indicated as #1), Cdc20 mouse monoclonal antibody (MAB3775; Millipore; clone AR12, indicated as #2), Cdc20 T70 and T59 phosphorylation-specific antibodies rabbit polyclonal antibody [raised against peptides CSKVQT(Tp)PSKPG and CRTPGR(Tp)PGKSS; Moravian Biotechnology; reference 22], APC3 T447p rabbit polyclonal [raised against Peptides CGKISTI(Tp)PQIQAF; Moravian Biotechnology], anti-phospho-histone H3 (Ser 10) rabbit polyclonal antibody (1:1,000; 06–570; Millipore), APC4 mouse monoclonal antibody (1:500; Moravian Biotechnology; clone CIV 1.1), APC3 mouse monoclonal antibody (1:500; Moravian Biotechnology), Mad2 rabbit polyclonal antibody (1:500; A300-300A; Bethyl Laboratories), Bub3 mouse monoclonal antibody (1:500; 611731; BD Biosciences), BubR1 rabbit polyclonal antibody (1:1,000; A300-995A; Bethyl Laboratories), and BubR1 mouse monoclonal antibody (1:500; Biotech Research and Innovation Centers; raised against TPR domain). Antibodies raised in goats against mouse or rabbit IgG coupled to IRDye 800CW or 680RD were used as secondary antibodies (926–32210 and 926–68071; Li-Cor Biosciences).

RNAi and plasmid transfection

Endogenous proteins were depleted using RNAi max from Life Technologies according to the manufacturer's instructions: Cdc20 (5′-CGAAAUGACUAUUACCUGA-3′; siRNA ID s2748; Thermo Fisher Scientific), B56 (oligoes as described in Foley et al., 2011), and BubR1 (5′GAUGGUGAAUUGUGGAAUAdTdT-3′; Sigma-Aldrich). In more detail, for live cell imaging, 50 µl of transfection mix with 1 µl siRNA Max and 0.25 µl siRNA oligo (stock concentration 10 µmol) in Optimem was added to 200 µl Optimem in eight-well Ibidi dishes with cells at a confluency of ∼80%. After 2 h of treatment, DMEM containing 20% FBS was added until medium was changed the next day.

Live cell imaging

Cells grown on eight-well slides (Ibidi) were cultured in complete DMEM and subjected to a double thymidine block. Cells were transfected with siRNA and plasmid between the two thymidine blocks. Two hours after release from the second thymidine block (or before filming), medium was changed to L-15 medium (Life Technologies) supplemented with 10% FBS (Hyclone) and nocodazole (30 ng/ml) when indicated. The slide was mounted on a Delta Vision Elite microscope (GE Healthcare) and cells were filmed for 16–24 h in 4–20-min intervals using a 40×, 1.35 NA, working distance (WD) 0.10 objective at 37°C. All data analysis was performed using softWoRx software (GE Healthcare). For statistical analysis, we analyzed the data in Prism using a Mann-Whitney test.

Purification of Cdc20 and APC4

Cdc20 and APC/C complexes were purified from cells after a double thymidine treatment protocol. HeLa cells (American Type Culture Collection) were seeded at 20% confluency on day 1 and treated with siRNA for 5 h when indicated. After 14–18 h in thymidine, cells were released for 8 h and, when indicated, transfected with plasmids. After a second 24-h thymidine treatment, cells were released into nocodazole (200 ng/ml) and harvested by mitotic shake-off. When indicated, cells were treated with RO3306 (5 or 10 µM) to force mitotic exit and collected at indicated times. Cells were lysed in lysis buffer (150 mM NaCl, 50 mM Tris-HCl [pH 7.8], 1 mM DTT, 0.1% NP-40) supplemented with PhosStop and Complete Mini (Roche). Cdc20 or APC/C complex was immunoprecipitated using a mouse monoclonal Cdc20 antibody (#1 or #2 as in the antibody section, #1 was used when not further specified) or mouse monoclonal APC4 antibody cross-linked to Protein G-Sepharose 4B (Life Technologies) for 1 h at 4°C. Precipitated protein complexes were washed in lysis buffer. Precipitated protein complexes were eluted with 4× LSB (Life Technologies).

Quantitative infrared Western

All cell lysates and immunoprecipatations were analyzed by Li-Cor Biosciences quantitative infrared Western blot technology. Proteins were separated by SDS-PAGE and blotted onto Immobilion FL membrane (Millipore). Membranes were incubated with indicated primary antibody and subsequently with IRDye 800 or 680 secondary antibodies (Li-Cor Biosciences). Membranes were scanned using the Odyssey Sa imaging system (Li-Cor Biosciences), and quantification was performed using the Odyssey Sa Application software (Li-Cor Biosciences).

Expression and purification of proteins

Proteins were produced as described previously in Hein et al. (2017). In short, full-length Arpp19 and derivatives thereof were cloned into pGEX-4T-1 to generate N-terminally GST-tagged fusion proteins. Constructs were transformed into BL21 (DE3) cells and expression was induced by addition of 0.5 mM IPTG at 37°C for 3 h. Expression for GST-Arpp19 was induced by addition of 0.5 mM IPTG overnight at 18°C. Bacterial pellets were resuspended in ice-cold lysis buffer (50 mM Tris-HCl [pH 7.4], 300 mM NaCl, 10% glycerol, 5 mM β-mercaptoethanol, 1 mM PMSF, and complete EDTA-free protease inhibitor cocktail tablets [Roche]) and lysed in an EmulsiFlex-C3 High Pressure Homogenizer (Avestin). Lysates were cleared at 26,200 *g* for 30 min at 4°C, and supernatants were incubated with prewashed Glutathione Sepharose 4 Fast Flow beads (GE Healthcare) for 90 min at 4°C with mixing. Beads were washed six times in ice-cold lysis buffer, and GST-fusion proteins were eluted at 22°C for 30 min, 1,250 rpm in elution buffer (50 mM Tris [pH 8.8], 300 mM NaCl, 10% glycerol, 5 mM β-mercaptoethanol, 20 mM reduced glutathione). Eluates were further purified by gelfiltration on a Superdex 75 10/300 GL column. For expression of MASTL, ten 15-cm dishes seeded with 10^7 cells per dish, were transfected with 15 µg FLAG-MASTL plasmid. Cells were collected 2 d after the transfection and FLAG-MASTL was purified by lysing cells in buffer L (350 mM NaCl, 50 mM Tris [pH 8.0], 0.05% NP-40). Following centrifugation, the lysate was incubated with 400 µl anti-FLAG beads (Sigma-Aldrich). Beads were washed with buffer L and FLAG-MASTL was eluted with buffer L containing 200 ng/µl FLAG peptide by incubating for 20 min at RT. 10% glycerol was added and FLAG-MASTL was snap-frozen and stored at −80°C.

Phosphorylation of GST-Arpp19 with MASTL

Thiophosphorylated GST-Arpp19 was generated as described previously (Hein et al., 2017). In short, purified GST, GST-Arpp19^{wt}, or GST-Arpp19^{S62A} was incubated with purified 3× FLAG-MASTL kinase in protein kinase buffer (50 mM Tris-Hcl [pH 7.5], 10 mM MgCl2, 0.1 mM EDTA, 2 mM DTT, 0.01% Brij 35) with 500 µM ATP and 1 µCi [γ-32P] ATP at 30°C for 30 min, or with 500 µM ATPγS at 30°C for 60 min for pull-down experiments.

Cell lysate phosphatase inhibition assay

The phosphatase inhibition assay was performed as described previously (Hein et al., 2017). In short, HeLa cells (American Type Culture Collection) were synchronized in mitosis with nocodazole (200 ng/ml) after double thymidine block. Cells were collected and washed with PBS. Lysis buffer (150 mmol NaCl, 25 mmol Tris, 0.1% NP-40, complete protease inhibitor) containing 1 mmol okadaic acid, 10 µg GST-Arpp19, or Nipp1 was added and immediately transferred to thermomixer for the indicated times at 600 rpm and 30°C. Ice-cold lysis buffer containing 2× PhosStop inhibitor tablets was added to stop the reaction. Lysis was cleared at 20,000 *g* for 15 min at 4°C and Cdc20 or APC4 was immune precipitated and samples analyzed by Western blot using the indicated antibodies. For mass spectrometry analysis, lysates were flash-frozen in liquid nitrogen after centrifugation.

Quantitative TMT phosphoproteomics analysis

LxxIxE and AxxAxE peptide-treated cell lysates were snap-frozen and proteins were acetone precipitated (Kruse et al., 2020). Precipitated proteins were digested overnight with trypsin (1:100 wt/wt) at 37°C. Digests were desalted using C_{18} solid-phase extraction cartridges (Thermo Fisher Scientific) and dried by vacuum centrifugation. Phosphopeptides were enriched in these samples using High-Select Fe-NTA Phosphopeptide Enrichment Kit according to the manufacturer's protocol (Thermo Fisher Scientific). Phosphopeptides were resuspended in 133 mM Hepes (Sigma-Aldrich), pH 8.5, and tandem mass tag (TMT) reagent (Thermo Fisher Scientific) stored in dry acetonitrile (Burdick & Jackson) was added, followed by vortexing to mix the reagent and peptides. After 1 h at RT, an aliquot was withdrawn to check for labeling efficiency while the remaining reaction was stored at −80°C. Once labeling efficiency was confirmed to be at least 95%, each reaction was quenched with ammonium bicarbonate for 10 min, mixed, acidified with 20% trifluoroacidic acid, and desalted. The desalted multiplex was dried by vacuum centrifugation and separated by offline pentafluorophenyl-based reversed-phase HPLC fractionation as previously described (Grassetti et al., 2017).

TMT-labeled samples were analyzed on an Orbitrap Fusion (Senko et al., 2013) mass spectrometer (Thermo Fisher Scientific) equipped with an Easy-nLC 1000 (Thermo Fisher Scientific). Peptides were resuspended in 8% methanol/1% formic acid across a column (45-cm length, 100-µm inner diameter, ReproSil, C_{18} AQ 1.8 µm 120 Å pore) pulled in-house across a 2-h gradient from 3% acetonitrile/0.0625% formic acid to 37% acetonitrile/0.0625% formic acid. The Orbitrap Fusion was operated in data-dependent, SPS-MS3 quantification mode (McAlister et al., 2014; Ting et al., 2011) wherein an Orbitrap MS1 scan was taken (scan range = 350–1,200 m/z; R = 120 K; AGC target = 3e5; max ion injection time = 100 ms). Followed by data-dependent Orbitrap trap MS2 scans on the most abundant precursors for a duration of 3 s. Ion selection; charge state = 2: minimum intensity 2e5; precursor selection range = 650–1,200 m/z; charge state 3: minimum intensity 3e5; precursor selection range = 525–1,200 m/z; charge state 4 and 5: minimum intensity 5e5). Quadrupole isolation = 0.7 m/z; R = 30 K; AGC target = 5e4; max ion injection time = 80 ms; CID collision energy = 32%). Orbitrap MS3 scans for quantification (R = 50 K; AGC target = 5e4; max ion injection time = 100 ms; HCD collision energy = 65%; scan range = 110–750 m/z; synchronous precursors selected = 5). The raw data files were

searched using COMET with a static mass of 229.162932 on peptide N termini and lysines and 57.02146 D on cysteines; and a variable mass of 15.99491 D on methionines and 79.96633 D on serines, threonines, and tyrosines against the target-decoy version of the human proteome sequence database (UniProt; downloaded 2/2020, 40,704 entries of forward and reverse protein sequences) and filtered to a <1% false discovery rate at the peptide level. Quantification of liquid chromatography–tandem mass spectrometry spectra was performed using in-house developed software (Kruse et al., 2020). Phosphopeptide intensities were adjusted based on total TMT reporter ion intensity in each channel and $\log_2$ transformed. P values were calculated using a two-tailed Student's *t* test assuming unequal variance.

Data availability

Raw MS data for the experiments performed in this study are available at MassIVE (MSV000086910) and PRIDE accession (PXD024245).

Online supplemental material

Fig. S1 provides additional data for the main figures. Data S1 provides the mass spectrometry screen for mitotic PP2A-B56 substrates.

Acknowledgments

Work at the Novo Nordisk Foundation Center for Protein Research is supported by grant NNF14CC0001, and J. Nilsson is supported by Danish Cancer Society Research Center grant R167-A10951-17-S2, Independent Research Fund Denmark grants DFF-4183-00388 and 8021-00101B, and Novo Nordisk Foundation grants NNF16OC0022394 and NNF18OC0053124. J.B. Hein was funded by Novo Nordisk Foundation grant NNF17OC0025404 and the Stanford Bio-X program. A.N. Kettenbach was supported by National Institutes of Health, National Institute of General Medical Sciences grant R35GM119455. The Orbitrap Fusion Tribrid mass spectrometer was acquired with support from National Institutes of Health grant S10-OD016212.

The authors declare no competing financial interests.

Author contributions: J.B. Hein performed all experiments, with the exception of all the mass spectrometry analysis, which was performed by A.N. Kettenbach and I. Nasa. D.H. Garvanska prepared samples for mass spectrometry together with J.B. Hein J. Nilsson coordinated the work and wrote the manuscript.

Submitted: 18 December 2020
Revised: 18 February 2021
Accepted: 25 February 2021

References

Alfieri, C., L. Chang, Z. Zhang, J. Yang, S. Maslen, M. Skehel, and D. Barford. 2016. Molecular basis of APC/C regulation by the spindle assembly checkpoint. *Nature.* 536:431–436. https://doi.org/10.1038/nature19083

Alfieri, C., S. Zhang, and D. Barford. 2017. Visualizing the complex functions and mechanisms of the anaphase promoting complex/cyclosome (APC/C). *Open Biol.* 7:170204. https://doi.org/10.1098/rsob.170204

Bancroft, J., J. Holder, Z. Geraghty, T. Alfonso-Pérez, D. Murphy, F.A. Barr, and U. Gruneberg. 2020. PP1 promotes cyclin B destruction and the metaphase-anaphase transition by dephosphorylating CDC20. *Mol. Biol. Cell.* 31:2315–2330. https://doi.org/10.1091/mbc.E20-04-0252

Barford, D. 2020. Structural interconversions of the anaphase-promoting complex/cyclosome (APC/C) regulate cell cycle transitions. *Curr. Opin. Struct. Biol.* 61:86–97. https://doi.org/10.1016/j.sbi.2019.11.010

Bastos, R.N., M.J. Cundell, and F.A. Barr. 2014. KIF4A and PP2A-B56 form a spatially restricted feedback loop opposing Aurora B at the anaphase central spindle. *J. Cell Biol.* 207:683–693. https://doi.org/10.1083/jcb.201409129

Chang, L.F., Z. Zhang, J. Yang, S.H. McLaughlin, and D. Barford. 2014. Molecular architecture and mechanism of the anaphase-promoting complex. *Nature.* 513:388–393. https://doi.org/10.1038/nature13543

Chao, W.C., K. Kulkarni, Z. Zhang, E.H. Kong, and D. Barford. 2012. Structure of the mitotic checkpoint complex. *Nature.* 484:208–213. https://doi.org/10.1038/nature10896

Cundell, M.J., L.H. Hutter, R. Nunes Bastos, E. Poser, J. Holder, S. Mohammed, B. Novak, and F.A. Barr. 2016. A PP2A-B55 recognition signal controls substrate dephosphorylation kinetics during mitotic exit. *J. Cell Biol.* 214:539–554. https://doi.org/10.1083/jcb.201606033

Di Fiore, B., N.E. Davey, A. Hagting, D. Izawa, J. Mansfeld, T.J. Gibson, and J. Pines. 2015. The ABBA motif binds APC/C activators and is shared by APC/C substrates and regulators. *Dev. Cell.* 32:358–372. https://doi.org/10.1016/j.devcel.2015.01.003

Di Fiore, B., C. Wurzenberger, N.E. Davey, and J. Pines. 2016. The Mitotic Checkpoint Complex Requires an Evolutionary Conserved Cassette to Bind and Inhibit Active APC/C. *Mol. Cell.* 64:1144–1153. https://doi.org/10.1016/j.molcel.2016.11.006

Espert, A., P. Uluocak, R.N. Bastos, D. Mangat, P. Graab, and U. Gruneberg. 2014. PP2A-B56 opposes Mps1 phosphorylation of Knl1 and thereby promotes spindle assembly checkpoint silencing. *J. Cell Biol.* 206:833–842. https://doi.org/10.1083/jcb.201406109

Foley, E.A., M. Maldonado, and T.M. Kapoor. 2011. Formation of stable attachments between kinetochores and microtubules depends on the B56-PP2A phosphatase. *Nat. Cell Biol.* 13:1265–1271. https://doi.org/10.1038/ncb2327

Fujimitsu, K., and H. Yamano. 2020. PP2A-B56 binds to Apc1 and promotes Cdc20 association with the APC/C ubiquitin ligase in mitosis. *EMBO Rep.* 21:e48503. https://doi.org/10.15252/embr.201948503

Gharbi-Ayachi, A., J.C. Labbé, A. Burgess, S. Vigneron, J.M. Strub, E. Brioudes, A. Van-Dorsselaer, A. Castro, and T. Lorca. 2010. The substrate of Greatwall kinase, Arpp19, controls mitosis by inhibiting protein phosphatase 2A. *Science.* 330:1673–1677. https://doi.org/10.1126/science.1197048

Godfrey, M., S.A. Touati, M. Kataria, A. Jones, A.P. Snijders, and F. Uhlmann. 2017. PP2A^{Cdc55} Phosphatase Imposes Ordered Cell-Cycle Phosphorylation by Opposing Threonine Phosphorylation. *Mol. Cell.* 65:393–402.e3. https://doi.org/10.1016/j.molcel.2016.12.018

Grassetti, A.V., R. Hards, and S.A. Gerber. 2017. Offline pentafluorophenyl (PFP)-RP prefractionation as an alternative to high-pH RP for comprehensive LC-MS/MS proteomics and phosphoproteomics. *Anal. Bioanal. Chem.* 409:4615–4625. https://doi.org/10.1007/s00216-017-0407-6

Heim, A., A. Konietzny, and T.U. Mayer. 2015. Protein phosphatase 1 is essential for Greatwall inactivation at mitotic exit. *EMBO Rep.* 16:1501–1510. https://doi.org/10.15252/embr.201540876

Hein, J.B., and J. Nilsson. 2014. Stable MCC binding to the APC/C is required for a functional spindle assembly checkpoint. *EMBO Rep.* 15:264–272. https://doi.org/10.1002/embr.201337496

Hein, J.B., and J. Nilsson. 2016. Interphase APC/C-Cdc20 inhibition by cyclin A2-Cdk2 ensures efficient mitotic entry. *Nat. Commun.* 7:10975. https://doi.org/10.1038/ncomms10975

Hein, J.B., E.P.T. Hertz, D.H. Garvanska, T. Kruse, and J. Nilsson. 2017. Distinct kinetics of serine and threonine dephosphorylation are essential for mitosis. *Nat. Cell Biol.* 19:1433–1440. https://doi.org/10.1038/ncb3634

Hertz, E.P.T., T. Kruse, N.E. Davey, B. López-Méndez, J.O. Sigurðsson, G. Montoya, J.V. Olsen, and J. Nilsson. 2016. A Conserved Motif Provides Binding Specificity to the PP2A-B56 Phosphatase. *Mol. Cell.* 63:686–695. https://doi.org/10.1016/j.molcel.2016.06.024

Herzog, F., I. Primorac, P. Dube, P. Lenart, B. Sander, K. Mechtler, H. Stark, and J.M. Peters. 2009. Structure of the anaphase-promoting complex/cyclosome interacting with a mitotic checkpoint complex. *Science.* 323:1477–1481. https://doi.org/10.1126/science.1163300

Holder, J., E. Poser, and F.A. Barr. 2019. Getting out of mitosis: spatial and temporal control of mitotic exit and cytokinesis by PP1 and PP2A. *FEBS Lett.* 593:2908–2924. https://doi.org/10.1002/1873-3468.13595

Izawa, D., and J. Pines. 2015. The mitotic checkpoint complex binds a second CDC20 to inhibit active APC/C. *Nature.* 517:631–634. https://doi.org/10.1038/nature13911

Kim, T., P. Lara-Gonzalez, B. Prevo, F. Meitinger, D.K. Cheerambathur, K. Oegema, and A. Desai. 2017. Kinetochores accelerate or delay APC/C activation by directing Cdc20 to opposing fates. *Genes Dev.* 31: 1089–1094. https://doi.org/10.1101/gad.302067.117

Kimata, Y., J.E. Baxter, A.M. Fry, and H. Yamano. 2008. A role for the Fizzy/Cdc20 family of proteins in activation of the APC/C distinct from substrate recruitment. *Mol. Cell.* 32:576–583. https://doi.org/10.1016/j.molcel.2008.09.023

Kruse, T., G. Zhang, M.S. Larsen, T. Lischetti, W. Streicher, T. Kragh Nielsen, S.P. Bjørn, and J. Nilsson. 2013. Direct binding between BubR1 and B56-PP2A phosphatase complexes regulate mitotic progression. *J. Cell Sci.* 126:1086–1092. https://doi.org/10.1242/jcs.122481

Kruse, T., N. Biedenkopf, E.P.T. Hertz, E. Dietzel, G. Stalmann, B. López-Méndez, N.E. Davey, J. Nilsson, and S. Becker. 2018. The Ebola Virus Nucleoprotein Recruits the Host PP2A-B56 Phosphatase to Activate Transcriptional Support Activity of VP30. *Mol. Cell.* 69:136–145.e6. https://doi.org/10.1016/j.molcel.2017.11.034

Kruse, T., S.P. Gnosa, I. Nasa, D.H. Garvanska, J.B. Hein, H. Nguyen, J. Samsøe-Petersen, B. Lopez-Mendez, E.P.T. Hertz, J. Schwarz, et al. 2020. Mechanisms of site-specific dephosphorylation and kinase opposition imposed by PP2A regulatory subunits. *EMBO J.* 39:e103695. https://doi.org/10.15252/embj.2019103695

Labit, H., K. Fujimitsu, N.S. Bayin, T. Takaki, J. Gannon, and H. Yamano. 2012. Dephosphorylation of Cdc20 is required for its C-box-dependent activation of the APC/C. *EMBO J.* 31:3351–3362. https://doi.org/10.1038/emboj.2012.168

Lara-Gonzalez, P., F.G. Westhorpe, and S.S. Taylor. 2012. The spindle assembly checkpoint. *Curr. Biol.* 22:R966–R980. https://doi.org/10.1016/j.cub.2012.10.006

Lischetti, T., G. Zhang, G.G. Sedgwick, V.M. Bolanos-Garcia, and J. Nilsson. 2014. The internal Cdc20 binding site in BubR1 facilitates both spindle assembly checkpoint signalling and silencing. *Nat. Commun.* 5:5563. https://doi.org/10.1038/ncomms6563

Ma, S., S. Vigneron, P. Robert, J.M. Strub, S. Cianferani, A. Castro, and T. Lorca. 2016. Greatwall dephosphorylation and inactivation upon mitotic exit is triggered by PP1. *J. Cell Sci.* 129:1329–1339. https://doi.org/10.1242/jcs.178855

McAlister, G.C., D.P. Nusinow, M.P. Jedrychowski, M. Wühr, E.L. Huttlin, B.K. Erickson, R. Rad, W. Haas, and S.P. Gygi. 2014. MultiNotch MS3 enables accurate, sensitive, and multiplexed detection of differential expression across cancer cell line proteomes. *Anal. Chem.* 86:7150–7158. https://doi.org/10.1021/ac502040v

McCloy, R.A., B.L. Parker, S. Rogers, R. Chaudhuri, V. Gayevskiy, N.J. Hoffman, N. Ali, D.N. Watkins, R.J. Daly, D.E. James, et al. 2015. Global Phosphoproteomic Mapping of Early Mitotic Exit in Human Cells Identifies Novel Substrate Dephosphorylation Motifs. *Mol. Cell. Proteomics.* 14:2194–2212. https://doi.org/10.1074/mcp.M114.046938

Mochida, S., S.L. Maslen, M. Skehel, and T. Hunt. 2010. Greatwall phosphorylates an inhibitor of protein phosphatase 2A that is essential for mitosis. *Science.* 330:1670–1673. https://doi.org/10.1126/science.1195689

Musacchio, A. 2011. Spindle assembly checkpoint: the third decade. *Philos. Trans. R. Soc. Lond. B Biol. Sci.* 366:3595–3604. https://doi.org/10.1098/rstb.2011.0072

Nijenhuis, W., G. Vallardi, A. Teixeira, G.J. Kops, and A.T. Saurin. 2014. Negative feedback at kinetochores underlies a responsive spindle checkpoint signal. *Nat. Cell Biol.* 16:1257–1264. https://doi.org/10.1038/ncb3065

Nilsson, J. 2019. Protein phosphatases in the regulation of mitosis. *J. Cell Biol.* 218:395–409. https://doi.org/10.1083/jcb.201809138

Pines, J. 2011. Cubism and the cell cycle: the many faces of the APC/C. *Nat. Rev. Mol. Cell Biol.* 12:427–438. https://doi.org/10.1038/nrm3132

Primorac, I., and A. Musacchio. 2013. Panta rhei: the APC/C at steady state. *J. Cell Biol.* 201:177–189. https://doi.org/10.1083/jcb.201301130

Rogers, S., D. Fey, R.A. McCloy, B.L. Parker, N.J. Mitchell, R.J. Payne, R.J. Daly, D.E. James, C.E. Caldon, D.N. Watkins, et al. 2016. PP1 initiates the dephosphorylation of MASTL, triggering mitotic exit and bistability in human cells. *J. Cell Sci.* 129:1340–1354. https://doi.org/10.1242/jcs.179754

Senko, M.W., P.M. Remes, J.D. Canterbury, R. Mathur, Q. Song, S.M. Eliuk, C. Mullen, L. Earley, M. Hardman, J.D. Blethrow, et al. 2013. Novel parallelized quadrupole/linear ion trap/Orbitrap tribrid mass spectrometer improving proteome coverage and peptide identification rates. *Anal. Chem.* 85:11710–11714. https://doi.org/10.1021/ac403115c

Sudakin, V., G.K. Chan, and T.J. Yen. 2001. Checkpoint inhibition of the APC/C in HeLa cells is mediated by a complex of BUBR1, BUB3, CDC20, and MAD2. *J. Cell Biol.* 154:925–936. https://doi.org/10.1083/jcb.200102093

Ting, L., R. Rad, S.P. Gygi, and W. Haas. 2011. MS3 eliminates ratio distortion in isobaric multiplexed quantitative proteomics. *Nat. Methods.* 8: 937–940. https://doi.org/10.1038/nmeth.1714

Varetti, G., and A. Musacchio. 2008. The spindle assembly checkpoint. *Curr. Biol.* 18:R591–R595. https://doi.org/10.1016/j.cub.2008.06.012

Vigneron, S., E. Brioudes, A. Burgess, J.C. Labbé, T. Lorca, and A. Castro. 2009. Greatwall maintains mitosis through regulation of PP2A. *EMBO J.* 28:2786–2793. https://doi.org/10.1038/emboj.2009.228

Wang, X., D.H. Garvanska, I. Nasa, Y. Ueki, G. Zhang, A.N. Kettenbach, W. Peti, J. Nilsson, and R. Page. 2020. A dynamic charge-charge interaction modulates PP2A:B56 substrate recruitment. *eLife.* 9:e55966.

Winkler, C., S. De Munter, N. Van Dessel, B. Lesage, E. Heroes, S. Boens, M. Beullens, A. Van Eynde, and M. Bollen. 2015. The selective inhibition of protein phosphatase-1 results in mitotic catastrophe and impaired tumor growth. *J. Cell Sci.* 128:4526–4537. https://doi.org/10.1242/jcs.175588

Yamaguchi, M., R. VanderLinden, F. Weissmann, R. Qiao, P. Dube, N.G. Brown, D. Haselbach, W. Zhang, S.S. Sidhu, J.M. Peters, et al. 2016. Cryo-EM of Mitotic Checkpoint Complex-Bound APC/C Reveals Reciprocal and Conformational Regulation of Ubiquitin Ligation. *Mol. Cell.* 63:593–607. https://doi.org/10.1016/j.molcel.2016.07.003

Yudkovsky, Y., M. Shteinberg, T. Listovsky, M. Brandeis, and A. Hershko. 2000. Phosphorylation of Cdc20/fizzy negatively regulates the mammalian cyclosome/APC in the mitotic checkpoint. *Biochem. Biophys. Res. Commun.* 271:299–304. https://doi.org/10.1006/bbrc.2000.2622

JCB

Supplemental material

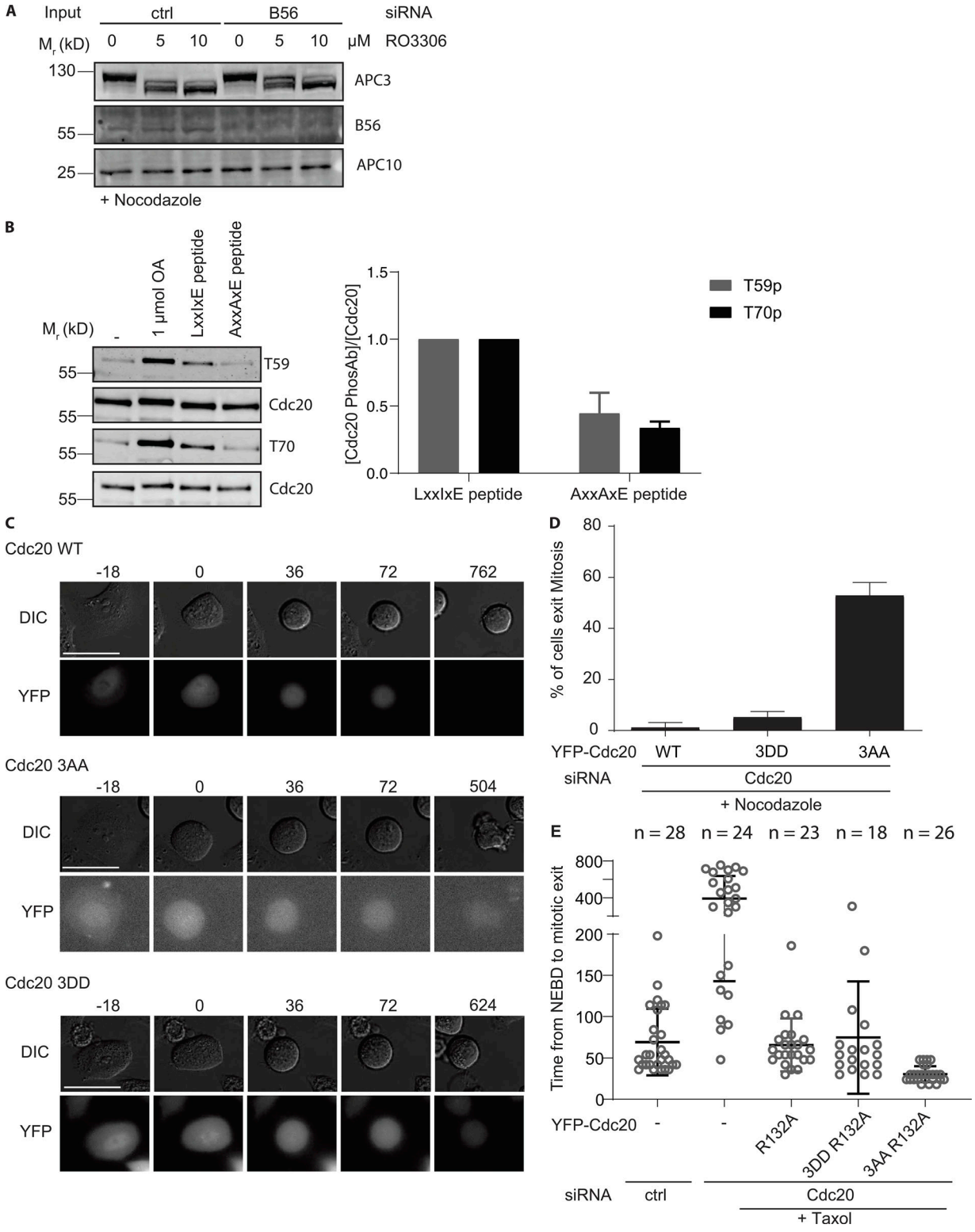

Figure S1. **Additional data supporting findings. (A)** Efficiency of B56 depletion related to Fig. 2 A. **(B)** Regulation of Cdc20 T59 and T70 by PP2A-B56 in a mitotic extract. The experimental setup was similar to Fig. 1 A. The pT59 and pT70 Cdc20 signal normalized to Cdc20 was set to 1 for the condition treated with LxxIxE peptide. **(C)** Representative images of live cell imaging of Hela cells depleted of endogenous Cdc20 and complemented with indicated forms of YFP-tagged Cdc20. Scale bar = 40 µm. **(D)** Quantification of cells that exit mitosis in the presence of nocodazole (30 ng/ml) during live cell imaging as in C from three independent experiments. Percentage of cells from three independent experiments (mean and SD indicated). **(E)** Hela cells depleted of endogenous Cdc20 and complemented with indicated forms of YFP-tagged Cdc20 in the presence of Taxol (25 nmol, when indicated). Time from NEBD to mitotic exit or end of filming from three independent experiments (each dot represents a single cell and *n* values are shown in the graph, red line indicates mean and standard deviation). DIC, differential interference contrast.

A supplemental dataset that provides the mass spectrometry screen for mitotic PP2A-B56 substrates is available online.